The influence of beam positioning on the weld ability of dissimilar welding joints with high alloy TRIP/TWIP steels

Lars Halbauer, Anja Buchwalder, Rolf Zenker, Horst Biermann

In dissimilar welded joints without filler materials, the positioning of the electron beam is one of the most crucial factors in controlling weld quality. Among other factors, the small beam diameter and a highly accurate positioning system mean that the electron beam can be advantageously used to join challenging materials. For this work, two dissimilar welding joints were successfully produced as a result of an optimised variation of the beam offset procedure. The microstructural characterisation was carried out with light optical and scanning electron microscopy procedures, such as EBSD and WDS. Hardness measurements and tensile tests with space-resolved temperature measurement were performed to determine the effect of the welding parameters on the mechanical properties of the joints produced. First, for welds involving a high alloy TWIP steel and the steel 42CrMo4, optimised beam positioning led to flawless joints with a tensile strength superior to that of the TWIP steel. Second, welded joints of a zirconia-reinforced TWIP steel with an as-cast TRIP steel could be produced free of pores and cracks within a small parameter window.

Влияние на позиционирането на лъча върху свойствата на заварката при различни заваръчни съединения със стомани, съдържащи високи стойности на TRIP / TWIP сплав (Ларс Халбайер, Аня Бучвалдер, Ролф Зенкер, Хорст Биерман). *При заваряване на различни материали, без да се използва запълващи материали, позиционирането на електронния лъч се явява един от най-важните фактори, определящи качеството на получените заварки. Заедно с другите фактори като малкият диаметър на лъча и високата точност на позициониращата система, електронният лъч може да бъде успешно използван за свързване на трудно свързващи се материали. За целите на тази разработка, две нееднородни заваръчни съединения са получени в резултат на оптимизираната вариация на "offset"процедурата на лъч. Микроструктурните му характеристики бяха изследвани с процедури като EBSD и WDS на светлинно-оптични и електронните микроскопи. Проведено е измерване на твърдоста и тестовете за якост с точково измерване на температурата, за да се определи ефекта от заваръчните параметри върху механичните свойства на завареният съединения. Първо: за заварки съдържащи високи стойности на сплавта TWIP и стомана от вида 42CrMo4, оптимизирането на позицията на лъча води до безупречни заварки, с по-добра якост на опън от тази на стомана от вида TWIP. Второ: в малък работен диапазон могат да бъдат получени заваръчни съединения на подсилена с цирконий TWIP стомана и TRIP стомана, които нямат пори и пукнатини при малък параметричен диапазон.*

Introduction

Requirements in relation to cost efficiency and lightweight constructions (predominantly in the automotive industry) create an enormous pull effect on the joining processes necessary for producing dissimilar welding joints. Due to their high R_m x A_{80} ratio, high alloy TRIP and TWIP steels are predestined for applications that require materials with outstanding mechanical properties – especially energy-absorbing applications [1]. For further improvement of these properties, TRIP/TWIP steels can be combined with ZrO_2, which facilitates the performance of a phase transformation during deformation, leading to even higher energy absorption capacities [2]. In joints with very different joining materials – e. g. with respect to the tendency for porosity formation [3], or the chemical compositions – the crucial parameter for obtaining optimum weld quality is that of dilution (D). Depending on the level of dilution, the corrosion resistance [4], wear behaviour [5, 6], crack susceptibility [7] or mismatch [8] of the bead can be controlled. It was shown that the mechanical properties of joints with high alloy

TRIP/TWIP steels exhibit maximum performance with high-strength steels as joining partners [9]. Therefore, two different butt joints were produced in this research program: first, joints between a TWIP steel and a hardened and tempered steel, and second, butt joints between a particle-reinforced TWIP steel and an as-cast TRIP/TWIP steel.

Materials and methods

For the welding experiments, sheets with a thickness of 10 mm were used. All joints were ground to a surface roughness of $R_Z < 80\ \mu m$ to ensure a minimal gap between the joining partners. The materials used with the chemical compositions given in Table 1 were available in as-cast (16-7-6 + 16-7-9), hardened and tempered (QT, $42CrMo_4$) and/or powder metallurgical (PM, 16-7-7 + 10 % ZrO_2) forms. The PM materials were produced by pressing steel and ZrO_2 powder at 30 MPa for 30 min at 1250°C. This led to a very low degree of porosity (< 1 %).

The steels were welded with the parameters given in Table 1 and without either filler material or preheating. After welding, the samples were cut perpendicular to the welding direction, ground, polished and etched with 'Lichtenegger' etchant to enhance visualisation of the microstructure (light optical microscopy – Neophot 30). The distribution of alloying elements across the cross section was examined via WDS measurements every 0.01 mm over a distance of 1.5 mm left and right of the centre of the welding seam (i.e. 3 mm in total).

The level of dilution (D) for all joint geometries was measured on cross sections (cf. Fig. 1) in relation to the welding gap after equation 1.

$$D = \frac{area\ \ A}{area\ \ B}.100\% \quad (1)$$

Since the welding gap of the butt joints was not present after full penetration welding, samples with greater sheet thickness were welded with the same set of parameters and used to determine the welding gap position.

EBSD measurements using a testing procedure described by Weidner et al. [10] were carried out to determine the phase distribution within the welding seam (WS). Radiographic examinations were carried out on longitudinal cross sections with an acceleration voltage of 135 kV and an exposure time of 2 - 4 min.

Table 1

Chemical composition, initial state of materials prior to welding: PM: powder metallurgically produced material; HR: hot-rolled material

		Element/Substance concentration						
		[wt.-%]					*[vol.-%]*	*[ppm]*
Steel	**State**	**C**	**Cr**	**Mn**	**Ni**	**Si**	**ZrO_2**	**N**
16-7-7+Z	PM	0.053	15.7	7.58	7.02	1.4	10	432
16-7-6	as-cast	0.044	16.2	7.07	6.52	0.88	0	246
16-7-9	As-cast	0.05	16.5	6.16	9.37	0.70	0	-
42CrMo4	QT	0.41	1.01	0.86	0	0.35	0	-

Table 2

EB parameters for the joints produced. U_A: Acceleration voltage; I_B: Beam current; v: Welding velocity; OF: Oscillation figure; d_{Osc}: Diameter of oscillation figure

U_A [kV]	**I_B [mA]**	**v [mm/s]**	**OF**	**d_{Osc} [mm]**
80	50	15	circle	0.3

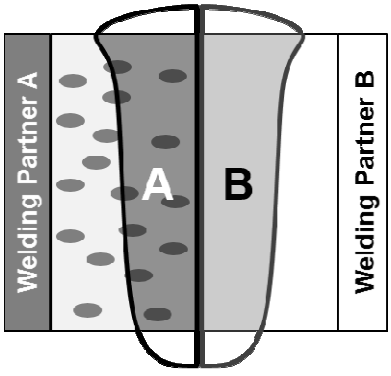

Fig. 1. Schematic diagram for the quantification of the dilution

The micro-hardness measurements were performed every 0.08 mm (Vickers, 100 - 300 N) perpendicular to the welding direction with an overall distance of ± 1.5 mm starting from the centre of the welding seam. Furthermore, mechanical tests were carried out according to DIN EN ISO 1002/2 (tensile tests for butt joints, B6 sample geometry). The initial strain rate was set to $2 \cdot 10^{-3}$ s^{-1} and the deformation of the samples was measured with an extensiometer.

For the evaluation of the temperature distribution across the sample surface during loading, all samples were painted with a completely opaque coat of black paint to ensure an emissivity of $\varepsilon = 0.96$. The samples were subsequently examined with a thermographic camera (InfraTec) with a sample rate of 27 frames per second.

Results and discussion

TWIP steel + QT steel

Macroscopic appearance

Independent of the beam offset used, the welding seams were free of pores and cracks. All joints had a distinct Y-shaped geometry and a seam width of 0.84 ± 0.03 mm. Head humping of 0.25 mm was evident. Due to the as-cast microstructure of the TWIP steel, a macroscopic heat-affected zone (HAZ) was only observable at the fusion line of the steel 42CrMo$_4$ (cf. Fig. *2*).

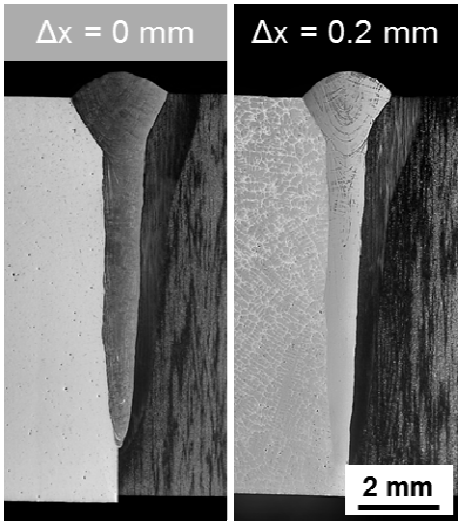

Fig. 2. The macroscopic appearance of the welding seam depending on the beam positioning relative to the welding gap (welding partners: 16-7-9 + 42CrMo4)

The hardness profile of the joints exhibited four different levels of hardness: The hardness levels of the two base materials, the hardness of the welding seam, and the hardness of the HAZ of the 42CrMo$_4$ (**Error! Reference source not found.**).

For joints without a beam offset, the hardness increased abruptly at the fusion line from the base level of the steel 16 – 7 – 9 to the hardness level of the welding seam. The enrichment of the welded zone with C and the depletion of Cr were observed (cf. WDS analysis, **Error! Reference source not found.**). At the fusion line to the steel 42CrMo$_4$, the chemical composition abruptly reached the level of the 42CrMo$_4$ base material, while the hardness increased to a maximum of 602 – 613 HV 0.3 at the fusion line and slowly decreased to the level of the base material (287 ± 24 HV 0.3).

For joints produced with a beam offset, a significant hardness increase from the TWIP steel to the welding seam was not detected, because the chemical composition corresponded strongly to the base material (16 – 7 – 9).

Overall, the hardness of the welding seam decreased with increasing beam offset (cf. Table 3). With a beam offset of 0.2 mm, the hardness of the welding seam was on the same level as that of the TWIP steel. The hardness of the HAZ of steel 42CrMo$_4$ was independent of the Ni content of the component material and the beam offset.

Table 3

*Micro-hardness of different joint areas (*Hardness of the HAZ represents the maximum hardness achieved)*

	Micro-hardness HV0.3			
Δx [mm]	*16-7-9*	*FZ*	*HAZ**	*42CrMo$_4$*
0	161±16	408± 16	602	287±24
0.2		178±13	613	

Microstructure of the welding seam

In joints produced without a beam offset, the welding seam exhibited a martensitic microstructure (Fig. 3, left). Retained austenite (RA) was found in the interdendritic region. The amount of RA decreased with increasing beam offset. With a beam offset of 0.2 mm, the welding seam was fully austenitic (Fig. 3, right).

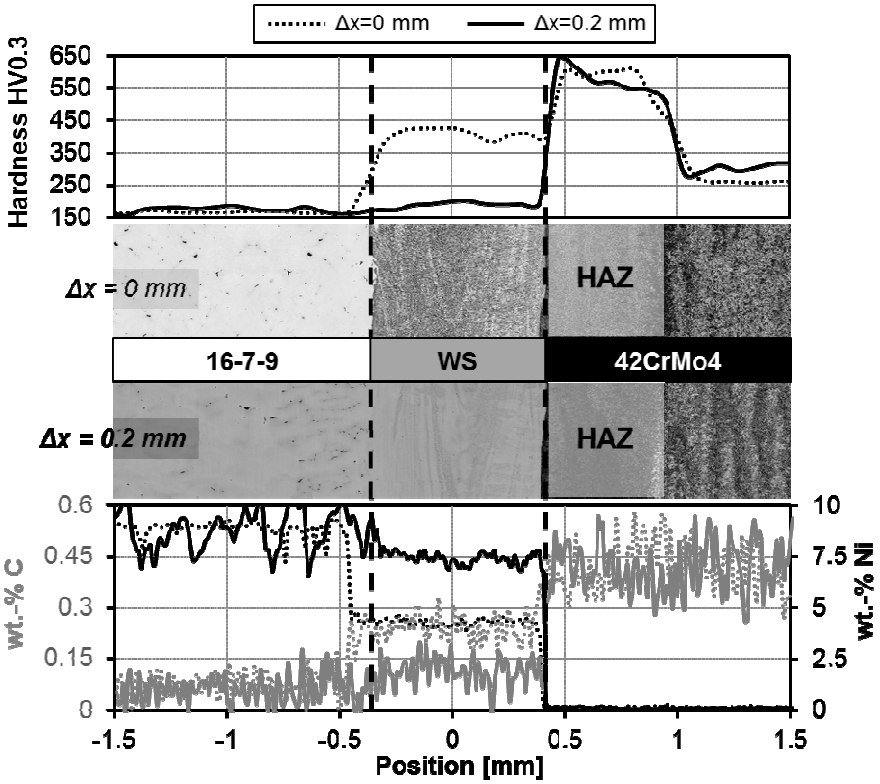

Fig.3. Micro-hardness profiles (top), macroscopic appearance (middle), and chemical composition according to WDS analysis (bottom) transverse to the welding direction as a function of the beam offset for a weld between 16-6-9 and 42CrMo4 steels.

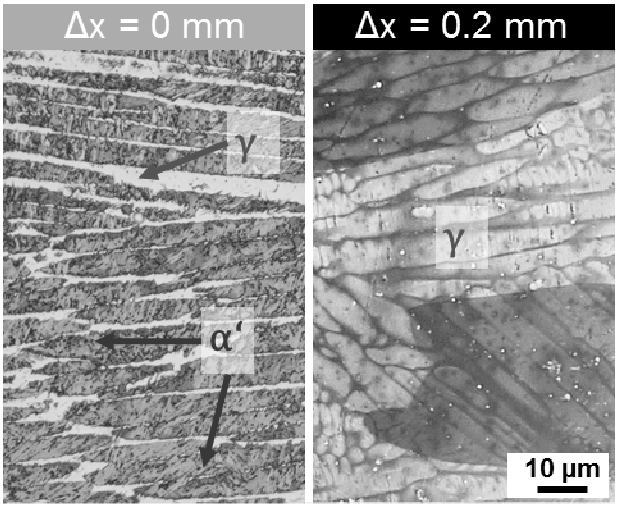

Fig. 3. The microstructure of the welding seam depended on the beam offset used. γ…retained austenite; α'…Martensite

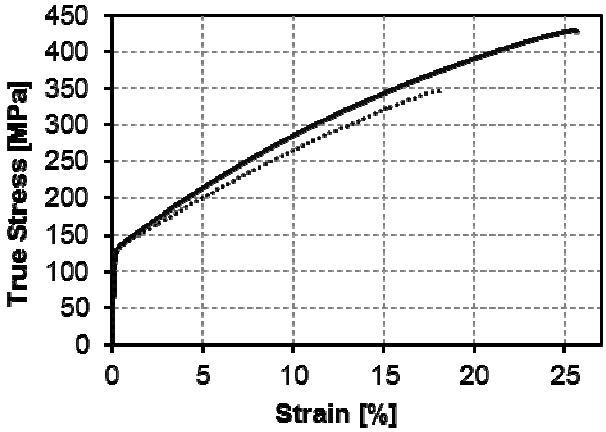

Fig. 4. Representative true stress-strain curves depended on the beam offset used

Mechanical behaviour

Overall, the mechanical behaviour was mainly influenced by the TWIP steel. Nevertheless, joints with a beam offset of 0.2 mm exhibited higher levels of strength and ductility (Fig. 4).

Independent of the beam offset applied, the samples exhibited a yield strength of ≈ 130 MPa, which represented the yield strength of the as-cast TWIP steel. Due to deformation after reaching the yield strength, strain hardening occurred. Since the TWIP effect is not based on a phase transformation like the TRIP effect, the shape of the stress-strain curve could not be distinguished from that of conventional high alloy steels. With increasing beam

offset, the uniform elongation ε_U increased from 19 ± 1 % (Δx = 0 mm) to 25 ± 0.5 % (Δx = 0.2 mm). The ultimate tensile strength σ_{UTS} increased from 386 ± 28 MPa (Δx = 0 mm) to 420 ± 11 MPa (Δx = 0.2 mm).

By means of space-resolved thermography, it could be shown that this behaviour was caused by a different strain distribution across the tensile samples during loading (Fig. 5). Without a beam offset during welding, the strain concentrated at the HAZ of the QT steel, leading to early failure. With a beam offset of 0.2 mm, the strain was concentrated within the ductile TWIP steel, leading to higher values of stress and strain.

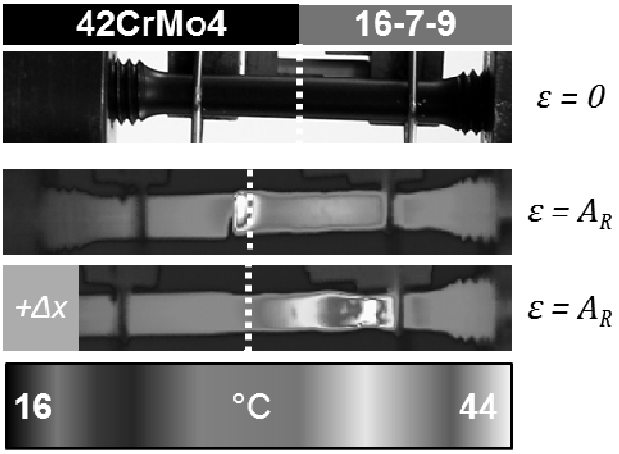

Fig. 5. Macroscopic appearance of the tested samples (ε= 0) and temperature distribution at rupture (ε= A_R) for different beam offsets. Dashed line: welding seam

Welding of ceramic-reinforced steel

The butt joints between the steels 16-7-6 and the ZrO_2–reinforced steel (16-7-7 + 10Zr) were also welded with different beam offsets to adjust the level of dilution. Three beam offsets were chosen, leading to the levels of dilution described in Table 4. All welds showed nearly parallel bead faces with minimal Y-shaping at 1 mm below the sheet surface, independent of the level of dilution (Fig. 6).

Table 4

Levels of dilution for the beam offsets used

Δx [mm]	0	0.3	0.4
D [%]	50	13	0.5

With decreasing levels of dilution, the size of the pores and cavities within the welding seam decreased. For Δx = 0 mm, the pores had the same width as the welding seam. For moderate levels of dilution (13 %, Δx = 0.3 mm) the pores were smaller and were located along the FL near the steel with ZrO_2. With nearly no dilution of the two welding partners (0.5 %, Δx = 0.4 mm), the welding seam was free of pores. In this case, the welding process could be described as a form of “braze-welding”.

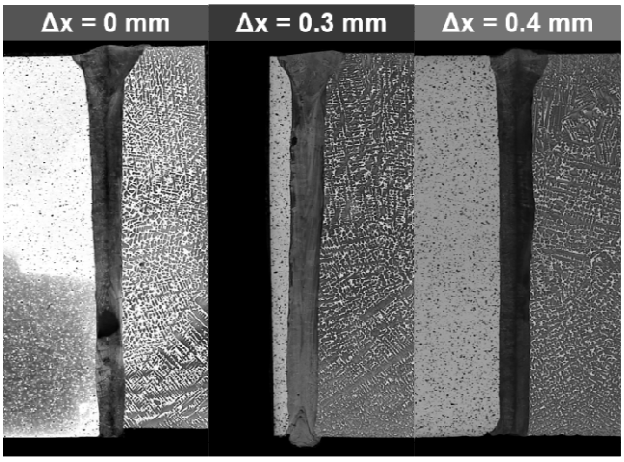

Fig. 6. Macrographs of the welded butt joints as a function of the beam offset used. White arrows indicate the location of pores/cavities

Mechanical properties

Due to the very similar chemical compositions of the base materials and the absence of carbon, the hardness of all joints did not change significantly from the base materials to the welding seam. When tested under uniaxial strain, no clear correlation between the mechanical properties and the level of dilution was found (cf. Fig. 7). For samples without beam offset and with maximum beam offset, the mechanical properties were nearly the same. The yield- and ultimate tensile strength were at the same level as the as-cast BM (16-7-6) [11]. In addition, the size of the pores decreased with increasing beam offset, and the worst mechanical properties were found for a beam offset of 0.3 mm (D = 13 %). The reason for the significantly decreased strain was the formation of a film of a non-metallic phase (MnO/MgO) at the interface between the upper third of the welding seam and the BM of the particle-reinforced steel (Fig. 8b, e). This film was not wettable for the molten metal of the bead. Therefore, the effective load-carrying diameter decreased drastically, leading to the significant deterioration of the mechanical properties. In the radiographs, more pores were found in samples welded without dilution (Fig. 8a). Though the samples broke alongside the non-metallic inclusions within the pores (Fig. 8d, also MnO/MgO), the mechanical properties were nearly unaffected. This was due to the high toughness of the welding seam, which compensated for the localised stress concentration at the pores up to high levels. Due to the refined microstructure of the welding seam, the joints with

0.5 % dilution broke within the coarse-grained BM (Fig. 8c, f). The parameter window for welds with this quality (free of pores) was very narrow, and amounted to ≈ 50 µm.

The formation of the non-metallic film mentioned could be proved by the EBSD investigations shown in Fig. 9. First, an area with a width of ≈ 100 µm and a high amount of misorientations of 60° (annealing twins) grew onto the base material of the zirconia-reinforced steel in an epitactic manner (Fig. 9b). Secondly, this area contained particles that were neither part of the matrix nor enriched with Zr, but enriched with Mn, Mg and O. It was concluded that these particles formed due to the evaporation of Mn from the matrix and of ZrO_2 from the particles inside the steel matrix, which was stabilised by MgO. Due to their high vapour pressure, Mg, Mn and O evaporate readily but cannot be carried out of the liquid melt fully. Since the process takes place only on the partially molten surface of the 16-7-7 + 10 ZrO_2, a phase boundary formed a compact layer after solidification.

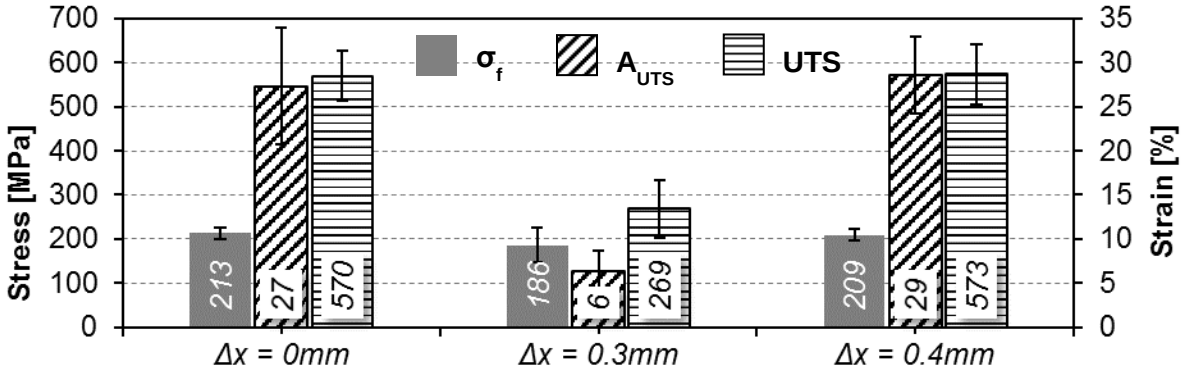

Fig. 7.Mechanical properties depended on the beam offset used

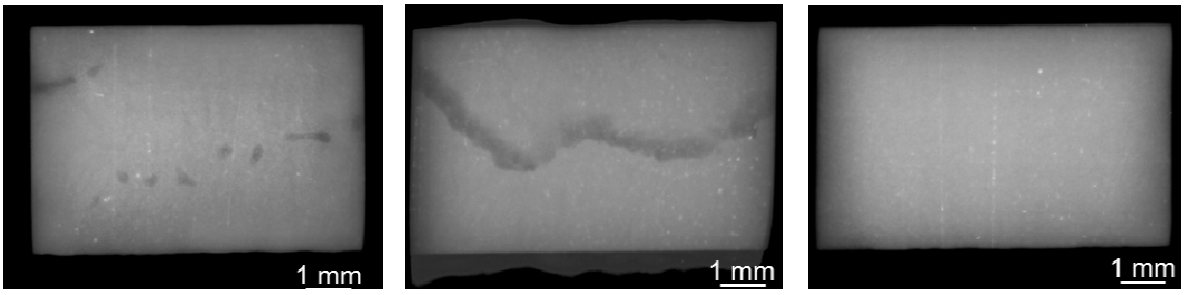

a) D = 50 %; Δx = 0 mm *b) D = 13 %; Δx = 0.3 mm* *c) D = 0.5 %; Δx = 0.4 mm*

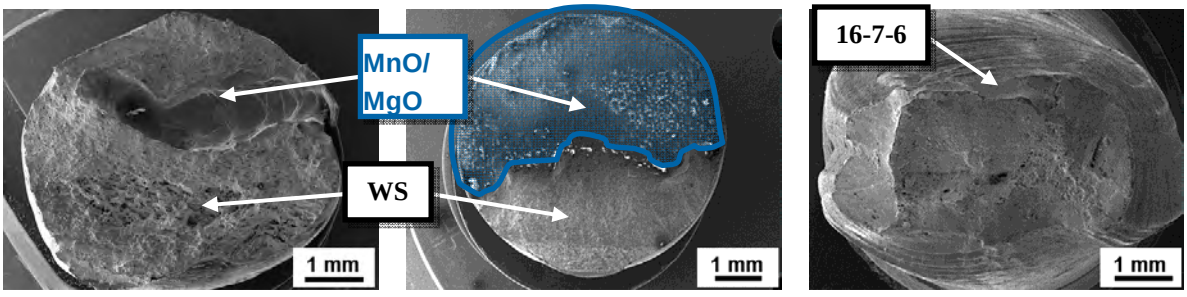

d) D = 50 %; Δx = 0 mm e) D = 13 %; Δx = 0.3 mm f) D = 0.5 %; Δx = 0.4 mm

Fig. 8. a-c): Radiographs of longitudinal cross sections before tensile tests, d-f): fracture surfaces of the welded and tensile-tested samples after rupture

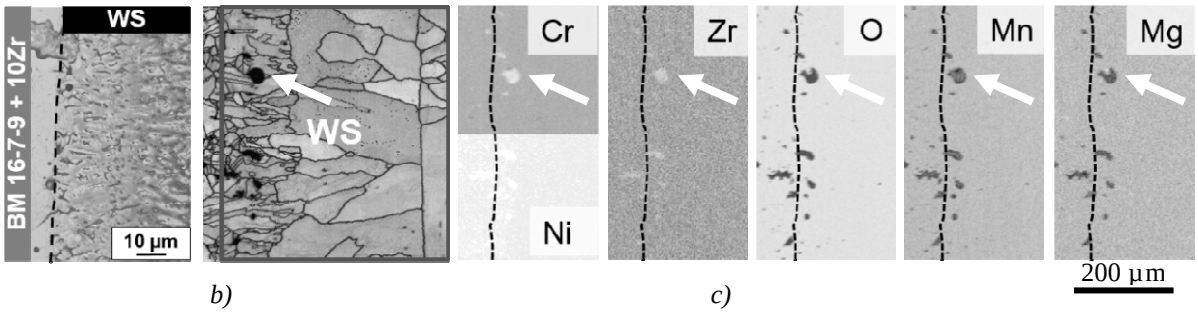

Fig. 9. EBSD measurements of the welded samples with D = 13 % and Δx = 0.3 mm. a) light optical overview b) misorientation map with misorintation angle θ (blue: 15° < θ < 60°, red: θ = 60°), c) EDS mapping for different alloying elements. White arrows indicate positions of MnO/MgO.

Summary and Conclusions

Two different types of dissimilar joints with varying beam offsets were successfully welded and tested. The welding joints between the TWIP steel 16-7-9 and the steel 42CrMo$_4$ were free of pores and cracks. With increasing beam offset towards the TWIP steel, the content of retained austenite in the primarily martensitic microstructure decreased. In the case of a beam offset of 0.2 mm, the hardness increase in the welding seam could be minimised because the chemical composition adapted to the high alloy base material. Independent of the beam offset used, a HAZ formed within the steel 42CrMo$_4$ (≈ 610 HV 0.3). The mechanical behaviour was mainly influenced by the high alloy base material and without a proper beam offset, rupture took place within the HAZ of the 42CrMo$_4$. When a beam offset of 0.2 mm was applied, the place of rupture was shifted towards the base material of the TWIP steel, leading to significantly higher levels of strength and elongation during the tensile tests. Furthermore, butt joints between the steels 16-7-7 + 10 % ZrO_2 and the as-cast 16-7-6 were successfully produced with an optimisation of the beam offset used. The beam offset is thus the critical parameter for producing welds of optimum quality. With increasing beam offset, the formation of pores could be suppressed due to the lower input of ZrO_2 in the melt pool. While a beam offset of Δx = 0.3 mm led to a significant deterioration of the mechanical properties, a beam offset of Δx = 0.4 mm produced welds free of pores and led to ductile failure in the base material of the as-cast 16-7-6.

Acknowledgements

The authors gratefully acknowledge the German Research Foundation (DFG) for supporting this work, which was carried out within the framework of the Collaborative Research Centre (SFB) 799, subproject A7. The authors would also like to thank K. Fischer for the SEM investigations and G. Schade for the realisation of the tensile tests.

REFERENCES

[1] A. Weiß, H. Gutte, A. Jahn, P.R. Scheller, Materialwissenschaft und Werkstofftechnik, *40 (8)*, 2009, 606. DOI: 10.1002/mawe.200800361.

[2] D. Ehinger, L. Krüger, U. Martin, C. Weigelt, C.G. Aneziris, Adv. Eng. Mater. 15 (7), 2013, 646. DOI: 10.1002/adem.201200345.

[3] L. Halbauer, A. Buchwalder, R. Zenker, H. Biermann, Weld World, 2016. DOI: 10.1007/s40194-016-0324-x.

[4] M. Nouri, A. Abdollah-zadeh, F. Malek, Journal of Materials Science and Technology, 23 (6), 2007, 817.

[5] K. Fritzsch, A. Buchwalder, R. Zenker, A. Jung, Corrosion Science 88, 2014, 109. DOI: 10.1016/j.corsci.2014.07.030.

[6] A. Jung, T. Sohr, R. Zenker, J. Lerche, K. Lerche, HTM, 70 (3), 2015, 135. DOI: 10.3139/105.110258.

[7] *M. Mangler, K. Rüthrich, R. Zenker, in Wissenschaftliche Zeitschrift der Hochschule Mittweida.*

[8] L. Halbauer, R. Zenker, A. Weidner, A. Buchwalder, H. Biermann, in JOM18 Conference Proceedings (Ed: Institute for the Joining of Materials) 2015.

[9] L. Halbauer, in JOM18 Conference Proceedings 2015.

[10] A. Weidner, A. Müller, A. Weiß, H. Biermann, Materials Science and Engineering: A 2013 (571), 68. DOI: 10.1016/j.msea.2013.02.008.

[11] A. Buchwalder, K. Rüthrich, R. Zenker, H. Biermann, Advanced Engineering Materials, 15 (7), 2013, 566. DOI: 10.1002/adem.201200355.

Lars Halbauer *– He is currently working at the TU Bergakademie Freiberg, Institute of materials engineering, Germany.*

Dr.-Ing. Anja Buchwalder *– He is currently working at*

the TU Bergakademie Freiberg, Institute of materials engineering, Germany.

Prof. Dr.-Ing. habil. Rolf Zenker *–Was born in Ottendorf, former GDR, 1946. He received his doctorate degree in materials engineering at the Technical University Karl-Marx-Stadt (now Chemnitz), 1975, and his postdoctorale lecture qualifycation (habil.) at the Technical University Bergakademie Freiberg, 1986. He was department manager and managing director in different companies and institutes. Since 2003, he is honorary professor at the Technical University Bergakademie Freiberg and managing director of Zenker Consult (Mittweida) and operates as project manager R&D and consultant for materials technologies. His research interests are electron and laser beam technologies, heat treatment, and surface technologies.*

Tel.: +49 (3727) 613581;

e-mail: contact@zenker-consult.de

Prof. Dr.-Ing. habil. Horst Biermann *– He is currently working at the TU Bergakademie Freiberg, Institute of materials engineering, Germany.*